2010 NDIA GROUND VEHICLE SYSTEMS ENGINEERING AND TECHNOLOGY SYMPOSIUM
MODELING & SIMULATION, TESTING AND VALIDATION (MSTV) MINI-SYMPOSIUM
AUGUST 17-19 DEARBORN, MICHIGAN

MECHANICAL BEHAVIOR AND FATIGUE STUDIES OF RUBBER COMPONENTS USED IN TRACKED VEHICLES

H.R. Brown
J.L. Bouvard, PhD
D. Oglesby
E. Marin, PhD
D. Francis
A. Antonyraj, PhD
H. Toghiani, PhD
P. Wang, PhD
M.F. Horstemeyer, PhD
Center for Advanced
Vehicular Systems (CAVS)
Mississippi State University
Mississippi State, MS

M.P. Castanier, PhD
CASSI Analytics Group
US Army TARDEC
Warren, MI

ABSTRACT

In this study, a styrene butadiene rubber, which is similar to the rubber used in road wheel backer pads of tracked vehicles, was investigated experimentally under monotonic and fatigue loading conditions. The monotonic loading response of the material was obtained under different stress states (compression and tension), strain rates (0.001/s to 3000/s), and temperatures (-5C to 50C). The experimental data showed that the material exhibited stress state, strain rate and temperature dependence. Fatigue loading behavior of the rubber was determined using a strain-life approach for R=0.5 loading conditions with varying strain amplitudes (25 to 43.75 percent) at a frequency of 2 Hz. Microstructural analysis of specimen fracture surfaces was performed using scanning electron microscopy and energy dispersive x-ray spectroscopy to determine the failure mechanisms of the material. The primary failure mechanisms for both loading conditions were found to be the debonding of particles on the order of 50 to 200 μm.

INTRODUCTION

Rubber components in military vehicles must overcome extreme loading conditions due to the harsh service environment such as high temperature, high friction and complex loading [1]. Due to the harshness of environment, rubber components often fail prematurely, causing a vehicle to become unusable in the field.

Efforts have been aimed at studying the factors affecting the bushings, backer pads, road wheels and suspension of tracked military vehicles [1]. The components of focus in this study, road wheel backer pads, are failing in the field at mileages that are approximately one-half of the design target. Understanding the loss in strength under such harsh conditions is of prime importance in increasing the component life. Thus, the micromechanisms of deformation and failure of the material must first be established under different loading conditions so that material and fatigue models may be developed and implemented.

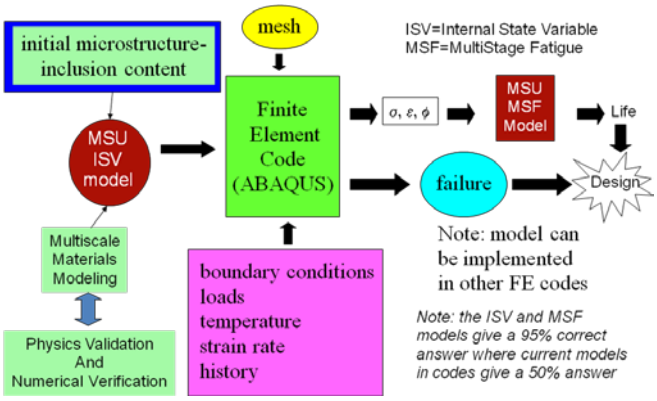

Figure 1: Methodology for using the history dependents ISV model implemented into a finite element code while using the MSF as a post-processor.

The overall modeling strategy is represented in Figure 1. Microstructural parameters from experiments are fed into a physics-based internal state variable model (ISV) in a finite element code. The ISV then provides inputs to a multistage fatigue (MSF) model which acts as a post-processer for determining fatigue life.

The purpose of this paper is to determine structure-property relations of rubber components of army tracked vehicles under monotonic and fatigue loading conditions in an effort to calibrate and validate the physics-based ISV material model for elastomers of [2] and the MultiStage Fatigue Model of [3]. Understanding the failure mechanisms and developing predictive capabilities for the track rubber can help predict component failure and improve its durability.

MATERIAL AND EXPERIMENTAL METHODS

Material

The track rubber used in the road wheel backer pads mainly consists of styrene butadiene rubber (SBR) along with reinforcing fillers, antiozonants and antidegradants. In the present document, an SBR similar to the track rubber materials is presented. SBR is an elastomeric copolymer consisting of styrene and butadiene, also called a random copolymer. Polystyrene is a tough hard plastic which gives its durability to this elastomers and polybutadiene is rubber, which gives rubber-like properties. SBR has good abrasion resistance and good aging stability when protected by additives. Various formulas of SBR are widely used in pneumatic tires, and gaskets.

Dynamic Mechanical Analysis (DMA)

DMA tests measure the evolution of the storage modulus, the loss modulus and loss tangent (tanδ) as a function of temperature or frequency. The glass transition temperature, T_g, was measured using the midpoint method [4], while other transitions were determined using procedures reported in the literature. DMA testing was performed on a TA Instrument Q900 Dynamic Mechanical Analyzer. The specimen geometry was rectangular with dimensions 1.5 in x 0.135 in x 0.06 in and used with DMA tensile clamps. The method was taken from ASTM D4065-01 [5]. The specimen was oscillated for a fixed frequency of 1 Hz for a range of temperatures chosen to include all the temperature transitions.

Monotonic Loading

Tension and compression tests were performed at room temperature, 50°C and -5°C at strain rates of 0.1/s, 0.01/s and 0.001/s. Compression tests were performed on an INSTRON 5882 mechanical load frame with a 50 kN load cell. Strain was measured using an INSTRON 25 mm extensometer; the extensometer was used in a feedback loop to control the strain rate of the tests. The specimen geometry was a cylinder with a height of 6.35 mm and a diameter of 12.7 mm [6]. This geometry is valid for both quasi-static and high rate experiments. Both sides of the platens were lubricated with moly paste and 0.01 inch Teflon plates to prevent friction from inducing an inhomogeneous stress-state in the specimen. Uniaxial tension tests were performed using an INSTRON 5869 mechanical load frame equipped with a 5kN load cell and pneumatic grips. The specimen geometry was taken from ASTM D412 [7] and scaled down in order for the specimens to fracture within the extension capabilities of the load frame (Figure 2). Local strain in the gage section was measured using a laser extensometer. The tests were performed in strain control, calculating strain from the extension of the crosshead. A correlation was made between strain rate calculated from extension and strain rate calculated from the laser extensometer so that the gage length was deformed at the given strain rate.

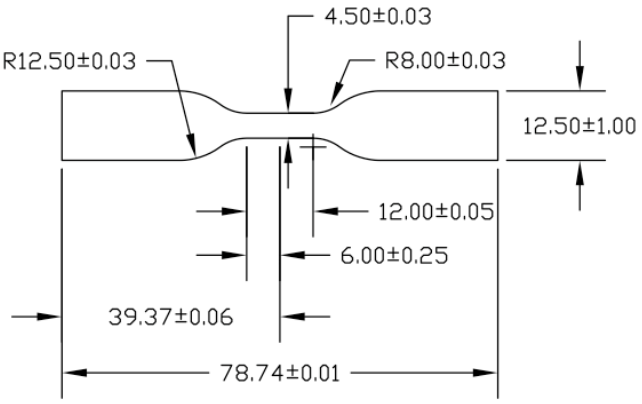

Figure 2: Tension specimen from ASTM D412.

For testing of the SBR in compression at high strain rates, an all polycarbonate Split Hopkinson Pressure Bar (SHPB) was used. The SHPB setup was comprised of 3 bars (striker, incident, and transmitter) with a strain gage on both the incident and transmitted bars. Specimen geometry and lubrication for SHPB testing were identical to quasi-static testing. The analysis of the data taken from the strain gages was conducted using the DAVID software package [8]. High rate tests were performed at a range of rates from 1200 to 3000/s.

Fatigue Loading

Fatigue tests were performed at room temperature on an MTS 858 servo-hydraulic load frame using the specimen geometry from Figure 2. As seen in Figure 3, a correlation was made between local strain in the specimen and

displacement of the crosshead using a laser extensometer, thus allowing displacement controlled tests at a specific strain amplitude [9]. To reduce uncertainty, the specimens were mounted in the load frame at the same position and the same initial grip-to-grip distance. Tests were performed under R=0.5 conditions at strain amplitudes of 43.75, 37.5, 32.5 and 25 percent at 2 Hz.

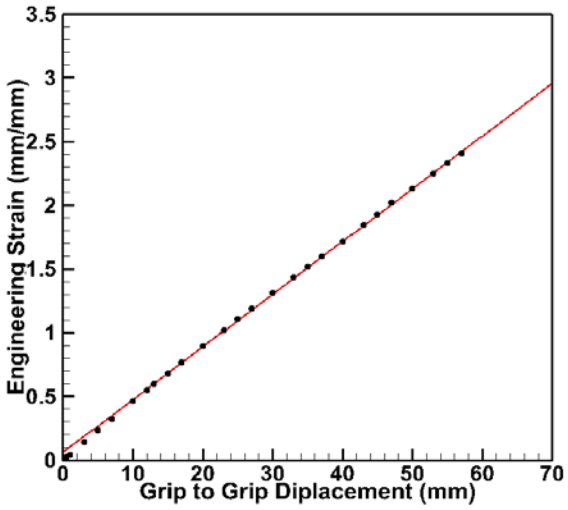

Figure 3: Correlation between engineering strain and grip-to-grip displacement.

Scanning Electron Microscopy (SEM)

The fracture surfaces from the failed monotonic and fatigue specimens tested at room temperature, mounted and sputter coated with gold and palladium for 100 seconds within 24 hours of fracture and viewed in the SEM within 48 hours of fracture to prevent creep of the fracture surfaces [10]. Energy dispersive x-ray spectroscopy (EDS) was performed on the particles present on the fracture surfaces.

RESULTS AND DISCUSSION

Viscoelasticity

The storage modulus curve for SBR (Figure 4) shows the presence of two transition temperatures. The first one related to the drop in the storage modulus corresponds to the glass transition temperature, which is determined from this curve at about -40°C (at 1 Hz) as reported in the literature [11-14]. A second transition temperature can be observed at -10°C. As described in [11-14], the mechanical properties of SBR are often improved with the use of filler such as carbon black [12] or blends such as poly (ethylene-co-vinyl acetate) (EVA) [14]. Thus, it is not clear here which component can be related to this damping in the loss modulus but it seems that the addition of an immiscible blend to SBR phase could be the origin of this second transition temperature.

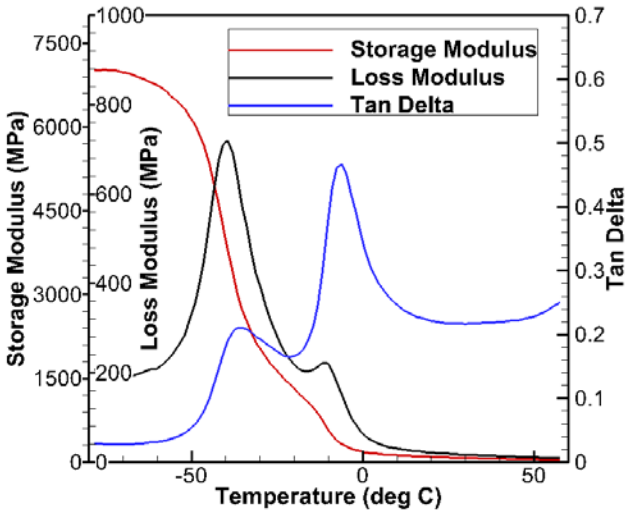

Figure 4: DMA temperature scan at 1 Hz.

Monotonic Loading

The SBR exhibited the characteristic elastomeric mechanical behavior of a relatively compliant response that stiffened with increasing strain. As shown in Figure 5, rate dependence was present in that the stress magnitude at a given strain increased as the applied strain rate was increased. As shown in Figure 6, temperature dependence was exhibited in that the material was softer and had a longer strain to failure at an elevated temperature. The recovery of the SBR under compressive loading was around 80% of total deformation.

The high rate stress-strain response of SBR in compression is shown in Figure 7. The compressive strain rates were 1200, 2000, 2600 and 3000/s. Rate dependence followed suit of the quasi-static rates in that the stress response to a strain increased with increasing rate.

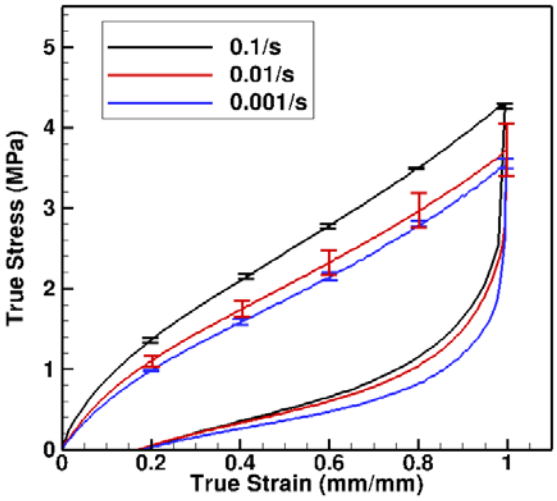

(a)

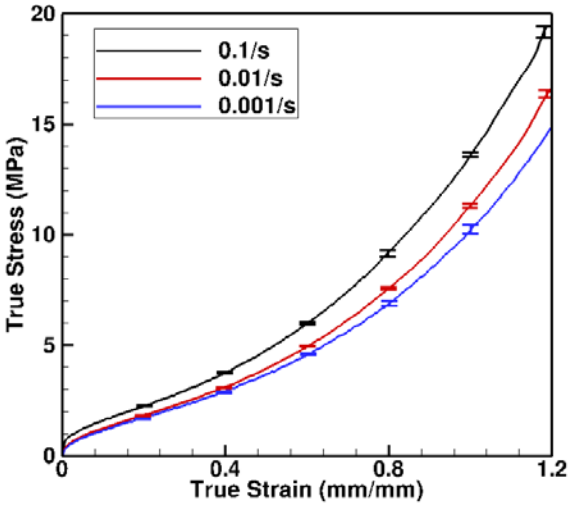

(b)

Figure 5: Rate dependence in (a) compression and (b) tension of SBR.

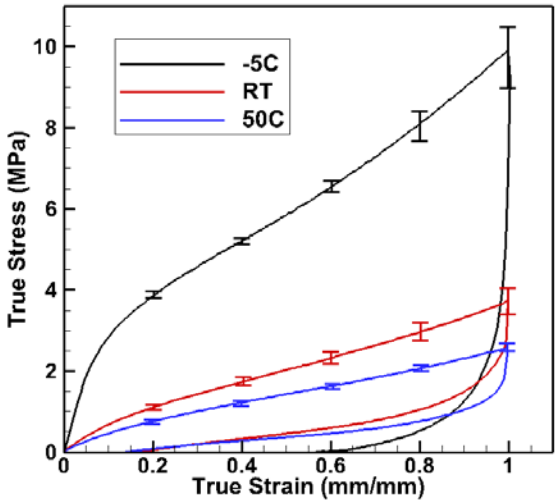

(a)

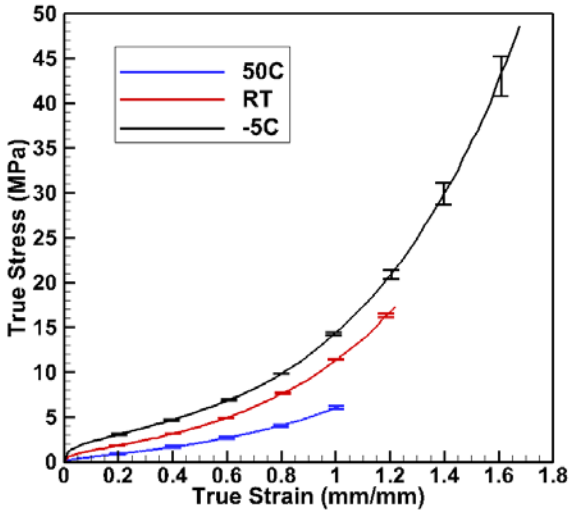

(b)

Figure 6: Temperature dependence in (a) compression and (b) tension of SBR.

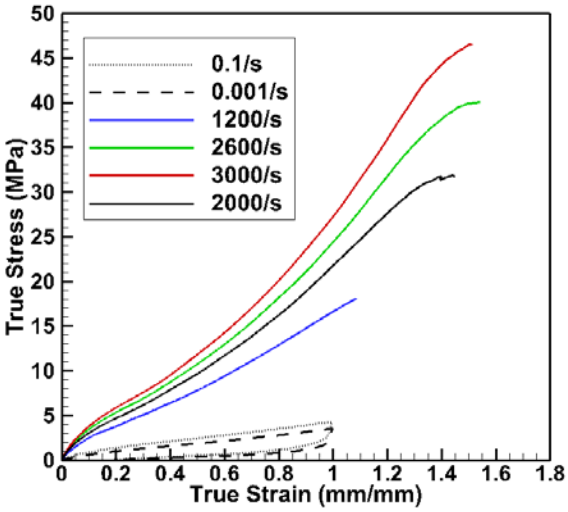

Figure 7: High rate testing of SBR.

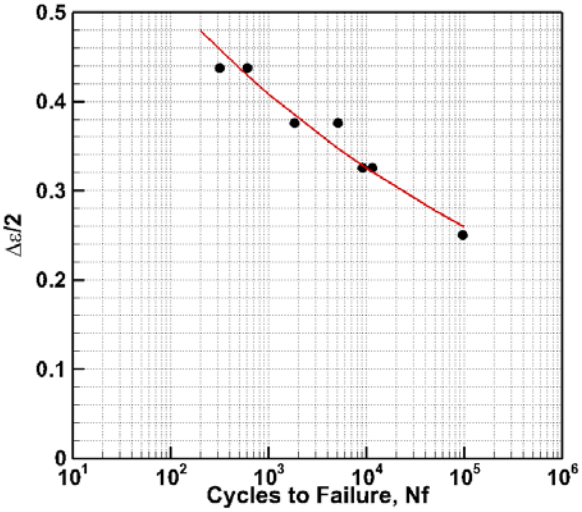

Figure 8: Strain-life for SBR from experiments conducted in displacement control at a frequency of 2 Hz and at R=0.5.

Fatigue Loading

The strain-life curve for SBR is shown in Figure 8. In order to provide some basic strain-life model capabilities, a power law fit of the strain-life results was obtained as in [15]. Thus, based on the experimental strain-life fatigue results, the following empirical equation (1) is presented:

$$\frac{\Delta\varepsilon}{2} = 0.8091\left(N_f\right)^{-0.099} \qquad (1)$$

where $\frac{\Delta\varepsilon}{2}$ is the strain amplitude and N_f is the cycles to failure. The empirical fit of the ε-N results are shown in Figure 6.

Typical hysteresis loops for first, middle and near last cycle are shown in Figure 9. The loops show that the SBR experienced significant softening due to the cyclic loading. This stress softening continues into the second half of the fatigue life as shown by the difference between the half and last cycles. The stress softening is believed to be due to the elastomer bonds breaking and particles debonding during the cyclic loading.

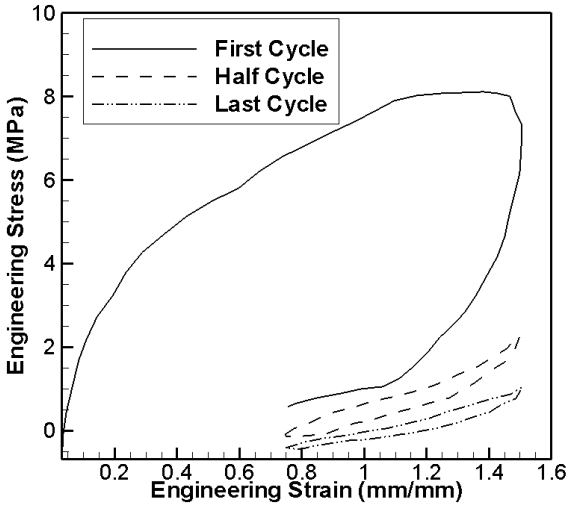

Figure 9: Typical hysteresis loops for the first, middle and near the last cycle at a strain amplitude of 0.375 and at R=0.5.

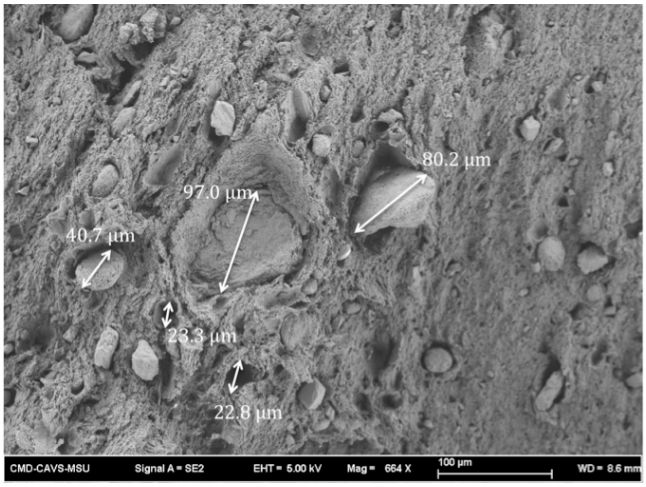

Figure 10: SEM image of fracture surface from room temperature tension at 0.1/s.

Figure 11: SEM image of fracture surface from room temperature tension at 0.001/s.

Microstructure

As seen in Figures 10 and 11, the major mechanism associated with monotonic failure was the decohesion of particles from the matrix. It was determined by EDS that the debonding of calcium carbonate particles on the order of 50 to 100 µm and agglomerates of aluminosilicate particles on the order of 50 to 200 µm led to failure.

As shown in the fractographs of failed fatigue specimens (Figure 12), the debonding of particles with a length scale of 50 to 200 µm initiated fatigue cracks. EDS determined that these particles were agglomerates of aluminosilicate. Cracks initiated on both the specimen surface (molded) and edge (cut). This reiterates that the cracks initiated from the debonding of particles initially present in the material rather than surface effects from the mold or die cutting [9].

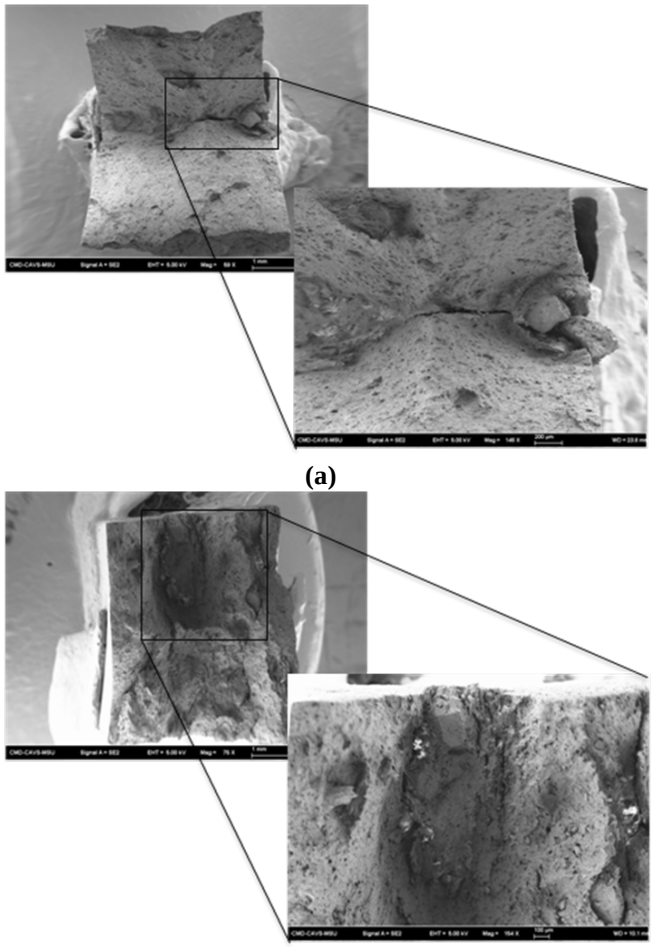

(a)

(b)

Figure 12: Fatigue fracture surfaces of specimens cycled with a strain amplitude of 37.5% (a) and 43.75% (b) at R=0.5, showing the crack-initiating particles.

Internal State Variable Model

A constitutive model [2] has been recently developed for amorphous thermoplastics using a thermodynamic approach with physically motivated internal state variables. The formulation follows current internal state variable methodologies used for metals and departs from the spring-dashpot representation generally used to characterize the mechanical behavior of polymers. In this effort, a model based on the same thermodynamic framework than [2] has been developed for elastomeric material to capture the time dependence exhibited by the material behavior. The 3D constitutive equations have been implemented in the FE code ABAQUS Explicit. The three dimensional equations

have been also reduced to the one-dimensional case to quantify the material parameters from monotonic compression test data at different applied strain rates.

Figure 13 displays the comparison between the compression tests at RT and the model predictions regarding SBR. We can observe that the model predicts with a good agreement the experimental testing during the loading. Both loading/unloading paths are well predicted by the constitutive equations as well. The material time dependence is also captured by the model.

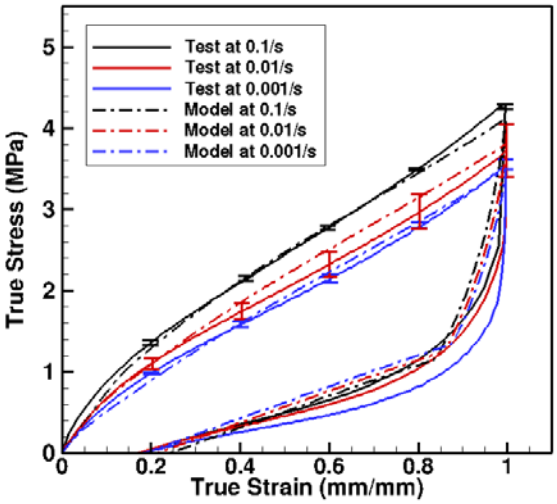

Figure 13: Comparison of model and experimental data in compression at RT.

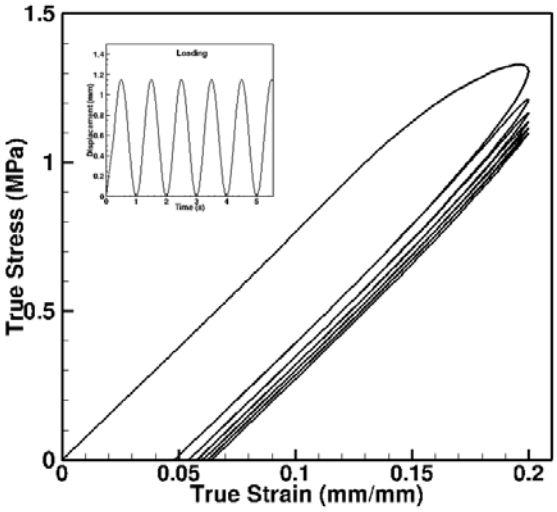

Figure 14: Model prediction under cyclic loading at 1 Hz.

Figure 14 displays the model response under cyclic loading at 1 Hz for a maximal strain level of 20% in compression. Notice that the material exhibits a significant hysteresis during the first cycle. The stress also exhibits some relaxation as the cycles evolve.

Fatigue Modeling

A MultiStage Fatigue (MSF) model developed in [3] has been applied to many types of aluminum, steel and magnesium. In the present effort, the MSF model is being extended to polymers. The MSF model considers fatigue of a material in 4 regimes as shown in Equation 2.

$$N_{total} = N_{inc} + N_{MSC} + N_{PSC} + N_{LC} \qquad (2)$$

where N_{total} is the total number of cycles to failure, N_{inc} is the number of cycles to incubate a fatigue crack, N_{MSC} is the microstructurally small crack growth, N_{PSC} is the physically small crack growth and N_{LC} is the long crack growth. Evolution equations describing the different stages of the cracking process of elastomers are being developed in this effort.

CONCLUSIONS

The following conclusions are drawn from this work:

- The storage modulus curve showed the presence of two transition temperatures, one of which was associated with the glass transition temperature.
- Rate dependence was present: the stress magnitude at a given strain increased as the applied strain rate was increased.
- Temperature dependence was exhibited: the material was softer and had a higher strain to failure at an elevated temperature.
- The debonding of calcium carbonate particles on the order of 50 to 100 μm caused failure under monotonic loading conditions.
- The MSF model equations need to be extended to elastomeric materials as well as calibrated and validated on SBR.
- Fatigue experiments must be conducted at lower strain amplitudes to give high cycle fatigue of the material.

ACKNOWLEDGEMENTS

The authors would like to acknowledge the support of the Center for Advanced Vehicular Systems (CAVS) at Mississippi State University (MSU) and TARDEC. They would also like to thank Bill Bradford and David Ostberg for the very productive discussions on this research.

REFERENCES

[1] D. Ostberg and B. Bradford, "Impact of Loading Distribution of Abrams Suspension on Track Performance and Durability", Proceedings of the 2009 Ground Vehicle Systems Engineering and Technology Symposium.

[2] J.L. Bouvard, D.K. Ward, D. Hossain, E.B. Marin, D.J. Bammann and M.F. Horstemeyer, "A General Inelastic Internal State Variable Model for Amorphous Glassy Polymers", Acta Mechanica, accepted 2010.

[3] D.L. McDowell, K. Gall, M.F. Horstemeyer and J. Fan. "Microstructure-based Fatigue Modeling of Cast A356-T6 Alloy." Engineering Fracture Mechanics, vol. 70, issue 1, pages 49-80, 2003.

[4]E.B. Marin, et al., "Material Database and Material Model Development for Polymeric Materials: Final Report", MSU.CAVS.CMD.2009-R0024, Supported by contract: Army W911NF-07-D-0001-0221, 2009.

[5] Standard Practice for Plastics: Dynamic Mechanical Properties: Determination and Report of Procedures, ASTM D4065-06, 2006.

[6] J. S. Bergstrom and M.C. Boyce, "Constitutive Modeling of the Large Strain Time-Dependent Behavior of Elastomers", Journal of the Mechanics and Physics of Solids, vol. 46, issue 5, pages 931-954, 1998.

[7] Standard Test Methods for Vulcanized Rubber and Thermoplastic Elastomers – Tension, ASTM D412 – 06ae2, 2006.

[8] Gary, G., DAVID Manual, http://www.lms. polytechnique.fr/dynamique/greef/web4034_david.html, 2005.

[9] W.V. Mars and A. Fatemi, "Fatigue Crack Nucleation and Growth in Filled Natural Rubber", Fatigue and Fracture of Engineering Materials and Structures, vol 26, pages 779-789, 2003.

[10] N.R. Choudhury and A. Bowmick, "Micromechanism of Failure of Thermoplastic Rubber", Journal of Materials Science, vol. 25, pages 2985-2989, 1990.

[11] R. Diaz de Leon, G. Morales, P. Acuna, J. Olivo, L.F. Ramos-DeValle, "Mechanical Behavior of High Impact Polystyrene Based on SBR Copolymers: Part I", Polmer Engineering Science, vol. 45, issue 9, pages 1288-1296, 2005.

[12] P. Konecny, M. Cerny, J. Voldanova, J.Malac and J. Simonik, "Dynamic Mechanical Properties of Filled Styrene Butadiene Rubber Compounds: Comparison of Tensile and Shear Data", Polymer Advaced Technology, vol. 18, pages 122-127, 2007.

[13] C. K. Radhakrishnan, Prajitha Kumari, A. Sujith, G. Unnikrishnan, "Dynamic Mechanical Properties of Styrene Butadiene Rubber and Poly (ethylene-co-vinyl acetate) Blends", Journal of Polymer Res, vol. 15, issue 2, pages 161-171, 2008.

[14] N. Sombatsompop, "Dynamic mechanical properties of SBR and EPDM vulcanisates filled with cryogenically pulverized flexible polyurethane foam particles", Journal of Applied Polymer Science, vol. 74, issue 5, pages 1129-1139, 1999.

[15] Y. Zhou and P. K. Mallick, "Fatigue Performance of an Injection Molded Talc-Filled Polypropylene", Polymer Engineering and Science, pages 510-516, 2005.